THE ASTRONOMICAL JOURNAL VOLUME 83, NUMBER 10 OCTOBER 1978

# HELIUM IONIZATION DRIVING IN BETA CEPHEI STARS

R. F. STELLINGWERF
Department of Physics and Astronomy, Rutgers University, Piscataway, New Jersey 08854
*Received 26 June 1978; revised 19 July 1978*

## ABSTRACT

In a series of nonadiabatic linear pulsation analyses, the destabilizing effect of the $He^+$ ionization *edge* (which is responsible for an opacity feature near $T = 1.5 \times 10^5$ K) is demonstrated. This mechanism is shown to be most effective in a region of the H–R diagram nearly coincident with that of the observed $\beta$ Cephei variables. Although actual instability is not obtained with standard models, it is shown that this could easily be due to approximations in the models and poor opacity resolution above $T = 10^5$ K. Slightly modified models that are presented do show an instability strip in good agreement with observed $\beta$ Cepheids.

## I. INTRODUCTION

In a recent study of $\delta$ Scuti stars (Stellingwerf 1976, 1978) a driving zone was found at a depth of $T = 1.5 \times 10^5$ K due to effects of the $He^+$ ionization edge. In $\delta$ Scuti models this zone is too deep to contribute significantly to the overall pulsational driving, but it was suggested that in hotter stars this driving zone could be effective. In the present paper we will show that this mechanism does tend to destabilize stellar models, and that this destabilization reaches a peak in a region of the H–R diagram very close to the position of observed $\beta$ Cephei stars.

At least eight theories of excitation have been proposed to account for the $\beta$ Cepheid instability (Cox 1976). None of these theories is currently considered completely satisfactory. These stars have properties quite distinct from variables in the classical Cepheid instability strip, and are much too hot to allow ordinary ionization zone destabilization. In spite of this, it has been noted by Aizenman and Weigert (1977) that the treatment of the $He^+$ ionization region and of the envelope opacity has a strong effect on stability results (in nonradial modes). The many complicated observed properties of these stars have been summarized by van Hoof 1970; Lesh and Aizenman 1973a, 1973b, 1974, 1975; and Jones and Shobbrook 1974. Beats are observed in some stars, as well as line broadening and doubling. This suggests that both low order radial and nonradial modes are present (Osaki 1976; Smith 1977).

Only the question of purely radial motion will be considered here. Previous investigations of this type have been presented by Davey (1973), by Cox and Tabor (1974), by Lesh and Aizenman (1974), and by Stothers (1976a, 1976b). No instability was found and no effective destabilizing mechanism was identified. The purpose of the present work is to demonstrate several points: (1) Even though standard models may be stable, a simple destabilizing mechanism exists; (2) this mechanism is most effective in models near the observed $\beta$ Cephei region; (3) the mechanism is the same as that noted in the $\delta$ Scuti survey—absorption by the $He^+$ ionization edge; and (4) only small changes in stellar opacities suffice to produce an actual instability strip.

## II. STANDARD MODELS

A series of static envelope models was constructed covering the outer 80% of the star by radius. Optical depth of the outer zone is chosen to be 0.01; zone size is a minimum of (0.02 in $\log T$) and (0.10 in $\log P$); the pressure criterion is only used in the outer few zones. This results in 350–400 zones in a typical model. Convection is ignored. The atmosphere is treated approximately by maintaining a diffusion treatment throughout. The opacity used is an analytic fit to the Los Alamos "King" tables [see Stellingwerf 1975a, and errata in Stellingwerf 1975b (footnote)]. These models are constructed similarly to sequences 1–4 of Stellingwerf (1978).

The models were analyzed in the linear nonadiabatic approximation (Castor 1971). The inner boundary of the envelope is assumed fixed, so possible destabilization due to nuclear reactions, convective core, or semiconvective zone is ignored. Complete details of the stability analysis are given in Stellingwerf (1975a).

A grid of 12 $M_\odot$ models was constructed with composition $X = 0.67$, $Y = 0.30$, $Z = 0.03$ at $M_{bol} = -5, -6, -7$ and $\log T_e = 4.1, 4.2, 4.3, 4.4$, and 4.5. An additional two 8 $M_\odot$ models were constructed at $M_{bol} = -3$ and $\log T_e = 4.1, 4.2$. Periods $\Pi_0$, $Q$ values, and kinetic-energy growth rates $\eta$ for these models are tabulated in Table I as sequences 2S, 3S, 4S, and 6S (*standard* sequences). Here $\eta$ represents fractional change in kinetic energy/period and factors of $10^{-N}$ are written as $(-N)$. All these models are stable. Higher modes were found to be much more stable, and are not shown. The periods and growth rates are generally in agreement with those given by Davey (1973).

 0004-6256/78/8310-1184$00.90  

TABLE I. Model parameters

| Model No. | $M/M_\odot$ | $M_{bol}$ | $\log T_e$ | $R/R_\odot$ | $\Pi_0(d)$ | $Q_0(d)$ | $\eta_0$ | $\eta_0'$ | Phase lag | $(\Delta R/R)/\Delta M_{bol}$ |
|---|---|---|---|---|---|---|---|---|---|---|
| 2.1S | 12 | −7 | 4.1 | 46.7 | 3.442 | 0.0374 | −1.9(−1) | −1.00 | −44 | 0.23 |
| 2.2S | 12 | −7 | 4.2 | 29.7 | 1.667 | 0.0357 | −5.6(−2) | −1.00 | −30 | 0.22 |
| 2.3S | 12 | −7 | 4.3 | 18.6 | 0.800 | 0.0348 | −1.7(−2) | −1.00 | −8 | 0.16 |
| 2.4S | 12 | −7 | 4.4 | 11.9 | 0.407 | 0.0346 | −6.4(−3) | −1.00 | −3 | 0.10 |
| 3.1S | 12 | −6 | 4.1 | 29.5 | 1.604 | 0.0348 | −1.3(−2) | −0.90 | −27 | 0.11 |
| 3.2S | 12 | −6 | 4.2 | 18.8 | 0.804 | 0.0344 | −2.5(−3) | −0.71 | −12 | 0.11 |
| 3.3S | 12 | −6 | 4.3 | 11.7 | 0.396 | 0.0344 | −7.3(−4) | −0.69 | 4 | 0.08 |
| 3.4S | 12 | −6 | 4.4 | 7.5 | 0.205 | 0.0347 | −2.6(−4) | −0.94 | 3 | 0.06 |
| 3.5S | 12 | −6 | 4.5 | 4.7 | 0.103 | 0.0352 | −6.5(−5) | −1.00 | −2 | 0.05 |
| 4.1S | 12 | −5 | 4.1 | 18.6 | 0.804 | 0.0349 | −4.9(−4) | −0.62 | −17 | 0.07 |
| 4.2S | 12 | −5 | 4.2 | 11.8 | 0.415 | 0.0355 | −6.8(−5) | −0.40 | −2 | 0.08 |
| 4.3S | 12 | −5 | 4.3 | 7.4 | 0.212 | 0.0368 | −1.8(−5) | −0.57 | 10 | 0.06 |
| 4.4S | 12 | −5 | 4.4 | 4.7 | 0.113 | 0.0384 | −4.5(−6) | −0.90 | 6 | 0.05 |
| 6.1S | 8 | −3 | 4.1 | 7.4 | 0.257 | 0.0361 | −9.5(−6) | −0.42 | −11 | 0.05 |
| 6.2S | 8 | −3 | 4.2 | 4.7 | 0.136 | 0.0377 | −1.1(−6) | −0.28 | 3 | 0.06 |
| 3.1N | 12 | −6 | 4.1 | 29.5 | 1.581 | 0.0343 | −1.9(−2) | −1.00 | −10 | 0.09 |
| 3.2N | 12 | −6 | 4.2 | 18.8 | 0.797 | 0.0341 | −5.1(−3) | −1.00 | −11 | 0.07 |
| 3.3N | 12 | −6 | 4.3 | 11.7 | 0.394 | 0.0342 | −1.1(−3) | −1.00 | −9 | 0.07 |
| 3.4N | 12 | −6 | 4.4 | 7.5 | 0.204 | 0.0346 | −2.6(−4) | −1.00 | −6 | 0.06 |
| 2.1E | 12 | −7 | 4.1 | 46.7 | 3.651 | 0.0397 | −2.8(−1) | −0.54 | −59 | 0.21 |
| 2.2E | 12 | −7 | 4.2 | 29.7 | 1.709 | 0.0366 | −4.6(−2) | −0.15 | −70 | 0.28 |
| 2.3E | 12 | −7 | 4.3 | 18.6 | 0.783 | 0.0340 | 3.1(−2) | 0.27 | −5 | 0.90 |
| 2.4E | 12 | −7 | 4.4 | 11.9 | 0.396 | 0.0336 | −2.4(−3) | −0.12 | 42 | 0.12 |
| 3.1E | 12 | −6 | 4.1 | 29.5 | 1.596 | 0.0346 | −3.3(−2) | −0.39 | −45 | 0.10 |
| 3.2E | 12 | −6 | 4.2 | 18.8 | 0.787 | 0.0336 | 1.0(−3) | 0.05 | −57 | 0.17 |
| 3.3E | 12 | −6 | 4.3 | 11.7 | 0.389 | 0.0337 | 5.7(−4) | 0.15 | 45 | 0.19 |
| 3.4E | 12 | −6 | 4.4 | 7.5 | 0.202 | 0.0342 | −2.1(−4) | −0.38 | 32 | 0.06 |
| 4.1E | 12 | −5 | 4.1 | 18.6 | 0.788 | 0.0342 | −8.6(−4) | −0.24 | −37 | 0.07 |
| 4.2E | 12 | −5 | 4.2 | 11.8 | 0.409 | 0.0350 | 6.2(−5) | 0.12 | −43 | 0.17 |
| 4.3E | 12 | −5 | 4.3 | 7.4 | 0.210 | 0.0365 | 1.9(−6) | 0.03 | 47 | 0.09 |
| 4.4E | 12 | −5 | 4.4 | 4.7 | 0.112 | 0.0378 | −5.1(−6) | −0.55 | 25 | 0.05 |
| 6.1E | 8 | −3 | 4.1 | 7.4 | 0.255 | 0.0357 | −1.1(−5) | −0.17 | −29 | 0.05 |
| 6.2E | 8 | −3 | 4.2 | 4.7 | 0.136 | 0.0376 | 7.6(−7) | 0.09 | −30 | 0.15 |

A glance at the work per zone, however, shows that these models generally do possess driving zones. Figure 1 shows the local $\oint PdV$ work plotted versus $\log T$ for three models in sequence 4S. The curves have been rescaled to comparable size. Note that temperature increases toward the *left,* so the stellar surface is at the *right.* Arrows indicate the location of opacity maxima near $T = 4 \times 10^4$ K ($He^+$ ionization zone, rightmost arrow), and $T = 1.5 \times 10^5$ K ($He^+$ ionization edge). It is seen that a strong driving zone is always present at $1.5 \times 10^5$ K, while the effect of the $He^+$ ionization zone is always negligible. As discussed by Cox and Giuli (1968, Sec. 27.7a), a driving zone is only effective if it occurs at optimum depth in the stellar envelope (the transition region between adiabatic and optically thin regions). Here, the $4 \times 10^4$ K ionization zone is always too shallow. In model 4.1S, it is seen that the deep driving zone is actually too deep to be very effective. This is also the situation in $\delta$ Scuti stars. In models 4.2S and 4.3S, however, the driving zone at $2 \times 10^5$ K clearly moves into the transition region and contributes maximal destabilization to the stellar envelope. It is clear that model 4.2S is very nearly unstable, but it is quite difficult to detect this tendency in the growth rates because of their strong variation with $T_e$ and $M_{bol}$.

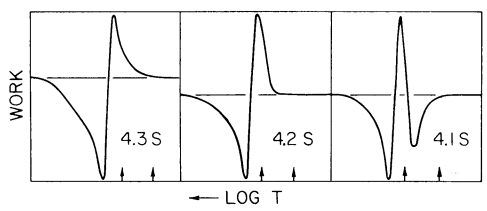


FIG. 1. Work per zone versus $\log T$ for three models in sequence 4S. The surface is at right; temperature increases to the left. Rightmost arrow in each case indicates the position of the $He^+$ ionization zone, second arrow indicates the opacity maximum near $1.5 \times 10^5$ K.

The driving zones appearing in Fig. 1 are caused by a slight inflection, or "bump," in the opacity tables near $1.5 \times 10^5$ K. This feature is discussed in Stellingwerf (1978, Appendix) where it is argued that it represents the coincidence of the frequency maximum of the radiation flux and the opacity edge due to $He^+$ ionization. The radiation field at this temperature is optimum for $He^+$ ionization; this produces an opacity bump even though $He^+$ is nearly completely ionized. Destabilization is caused by the variation of the opacity temperature

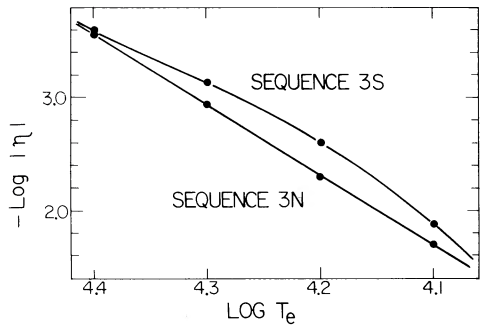


FIG. 2. Growth rate (log scale) versus effective temperature for sequence 3S (standard) and 3N (no opacity bump at $1.5 \times 10^5$ K).

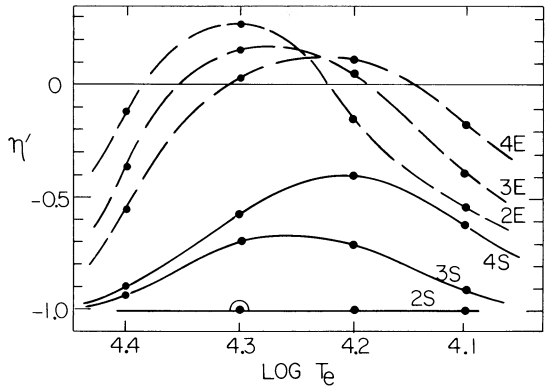


FIG. 3. Normalized growth rate $\eta'$ (see text) versus effective temperature for the model sequences as indicated.

derivative, and is therefore a type of "kappa mechanism," as discussed by Baker (1966). It was shown in Stellingwerf (1978) that this mechanism is more effective in *less* centrally condensed stars. It should be noted that an ordinary ionization zone near $2 \times 10^5$ K could also destabilize these stars (Cox 1965; Underhill 1966). Elements with the proper ionization potential (200–300 eV) are not abundant enough to be effective, but may contribute slightly.

Stothers (1976b) has investigated the destabilizing effect of the CNO features present at $\log T = 5.6$ and 5.8 in the Carson (1976) opacity tables. He finds that driving is produced by these features through a kappa-mechanism effect similar to that discussed above. These deeper opacity bumps have been shown to destabilize radial modes at higher masses (Stothers, 1976a); the $\beta$ Cephei models, however, were found to be stable. It is interesting that a driving zone at $\log T = 5.2$ was also present in Stothers's models (private communication), but was much weaker than the CNO driving.

To verify the cause of the instability, sequence 3 was recomputed with a modified opacity in which the "bump terms" were omitted (terms in $T^{2.5}$ and $T^{-10}$ in Eq. D3 of Stellingwerf 1975a). These models are given in Table I as sequence 3N. No hint of a driving zone is present in any of the N models. The growth rates for sequences 3S and 3N are shown on a logarithmic scale in Fig. 2. The destabilization is clearly seen. It extends over a limited interval in $T_e$ and at maximum reduces the dissipation to about half its former value.

The tendency toward destabilization clearly shown by the work curves in Fig. 1 can be quantified by defining a normalized growth rate $\eta'$ as follows: $\eta'$ is the normal growth rate $\eta = \int (\oint PdV)dm$ divided by $\int |\oint PdV| dm$. If $W_+$ (>0) represents the area under the positive portions of the work curve, and $W_-$ (<0) the total area of the negative portions, then $\eta' = (W_+ - W_-)/(W_+ + W_-)$. Note that $\eta' = 1.0$ if the entire envelope drives, and $\eta' = -1.0$ if the envelope is entirely dissipative. Values of $\eta'$ are listed in Table I and are plotted (solid lines) in Fig. 3. Sequence 2S has no driving regions, but comes closest at 2.3S, as indicated in the figure. It is seen that the instability increases at lower luminosities, and that maximal instability occurs at *lower $T_e$ for lower luminosites*. This trend is opposite to that of the classical Cepheid instability strip, but is exactly the trend observed in $\beta$ Cepheids.

The locus of maximum destabilization is plotted (short dashes) on the H–R diagram in Fig. 4. Also shown are locations of observed variables (taken from Lesh and Aizenman 1973a), the zero-age main sequence, a 12 $M_\odot$ evolutionary track for $Z = 0.03$, lines of constant period, and locations of all models discussed here (small circles). Figure 4 shows that the locus of destabilization runs parallel to the region occupied by observed variables, but

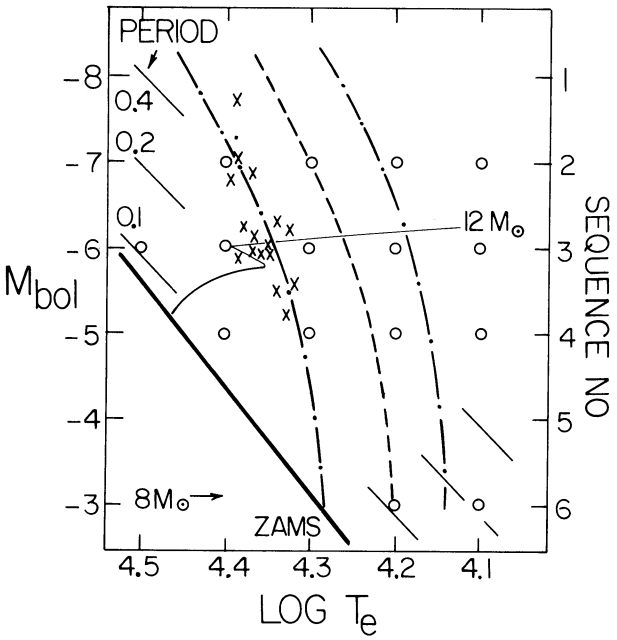


FIG. 4. H–R diagram showing the positions of observed $\beta$ Cepheids (X), models (o), line of maximum destabilization for the S models (dashed line), and the instability strip given by the E models (dot-dashed lines). Also shown are lines of constant period, an evolutionary track for a 12 $M_\odot$, $Z = 0.03$ model, the zero-age main sequence (ZAMS), and the sequence numbering scheme (at right).

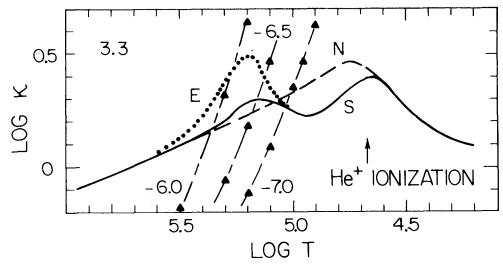


FIG. 5. Run of opacity versus temperature for models 3.3S, N, and E, as labeled. Triangles are opacity points taken directly from the King IVA table at densities of $\log\rho = -6.0, -6.5$, and $-7.0$, as indicated.

is shifted about 0.1 in $\log T_e$ toward the red. A shift of this magnitude could be due to uncertainties in the models or in the observations. Sequence 6S models (Table I) indicate the overall curvature of the instability region as shown in Fig. 4. This suggests that the negative slope is a high-luminosity effect caused by radiation pressure as found by Dziembowski (1978) in the upper Cepheid strip.

## III. ENHANCED OPACITY BUMP MODELS

In a recent study of Cepheid pulsation, Davis and Davison (1978, Fig. 4) compared a model using the analytic opacity formula used here with an otherwise identical model using the King IVA opacity tables directly. In the model considered, the agreement is excellent, but the fit underestimated the third local opacity maximum by about 50%. This discrepancy is caused by small changes in the structure of the model. Since this is precisely the opacity feature responsible for the destabilization discussed above, it appears possible that the bump may actually be underestimated in the present models, and it is therefore of interest to inquire whether a small opacity change would suffice to produce an actual instability. In this section several series of models will be discussed that show that this is in fact the case.

The opacity modification was accomplished by changing two terms in the original formula (Eq. D3 of Stellingwerf 1975a). The $T^{2.5}$ term was deformed quadratically upward above $T = 10^5$ K, and the $T^{-10}$ term was shifted upward in such a way as to maintain the intersection of the two terms (the bump position) at constant temperature. No change in opacity was made below $T = 10^5$ K or above $T = 4 \times 10^5$ K. The modified terms replaced the old terms in the interpolation formula, resulting in a smooth variation. Of course, the actual $He^+$ edge absorption is discontinuous in frequency and could be a complicated function of temperature as well. Absorption features of elements other than He are also present. Any small scale fluctuation would increase the destabilization.

The actual run of opacity in models 3.3S (standard), 3.3N (no bump), and 3.3E (enhanced bump) is shown in Fig. 5. In model 3.3S, the bump, which is barely noticeable in the opacity tables, appears as a distinct secondary maximum near $\log T = 5.2$. Note that the actual variation of the opacity is very small, but changes in the opacity derivatives, caused by structural adjustments in the model, are appreciable. Model 3.3N is similar to model 3.3S, but the secondary bump does not appear. Model 3.3E shows opacities magnified about 70% near $\log T = 5.2$. This modification should offset any error caused by the analytic interpolation. The magnitude of the correction is small in comparison with existing discrepancies in current opacity calculations [Magee, Merts, and Huebner (1975) found a factor of two change caused by the treatment of narrow line profiles, while Carson (1976) finds peaks differing by an order of magnitude near $\log T = 5.6$ and 5.8]. Also, newer opacities invariably show a more distinct feature at $\log T = 5.2$. On Fig. 5 the actual data point at $\log\rho = -6, -6.5$, and $-7$ in the King IVA table (Cox and Tabor 1974) have been plotted as triangles. It is seen that at $T = 10^5$ K the table switches to an extremely coarse grid spacing, so the actual shape of this feature is surely unresolved—not to mention any fine structure, cusps, etc. It is seen that the opacity is a sensitive function of both density and temperature in this region. Small wiggles in $\kappa(\rho,T)$ tend to be magnified in the model structure. For these reasons, we argue that the opacity modification shown for model 3.3E is not impossible, and is, perhaps, even reasonable.

All of the S models were recomputed with the enhanced bump, and are shown as E models in Table I. The normalized growth rates $\eta'$ are plotted with dashed lines in Fig. 3. An instability region of limited extent in effective temperature is present. This new instability strip is shown by dot-dashed lines on the H-R diagram, Fig. 4; it is completely consistent with the maximally destabilized S models. The instability strip extends to the main sequence near $\log T_e \approx 4.2$ (late B stars). Growth rates at lower luminosities are very small, but the large values of $\eta'$ indicate definite destabilization. It should be noted that the *width* of the strip depends on the degree of bump enhancement and is therefore completely arbitrary.

## IV. COMPARISON WITH OBSERVATIONS

As noted above, the instability strip found here is slightly redder than observed variables, the spectral types being B2–B4 as opposed to B1–B3 observed at $M_{bol} = -5$ to $-7$. Improved models could easily remove a shift of this magnitude. Recent observations have extended the observed instability region greatly (Sareyan *et al.* 1978; Smith 1977). Beardsley (1978) reports variability in the Pleiades as late as B6–B8. Further clarification of both models and observations is needed, but at this point the agreement shown in Fig. 4 must be considered very good. In particular, the negative slope, highly unexpected for an envelope ionization mechanism, matches the observed slope exactly.

Observed periods fall in the range 0.13–0.30 day. As shown in Fig. 4 the model periods at the observed positions are too large. On this basis Lesh and Aizenman (1974) concluded that first-overtone pulsations were indicated. The mechanism discussed in this paper does not admit overtone pulsations; higher modes are found to be strongly damped. Lesh and Aizenman, however, point out that their luminosities may be an upper limit. New luminosities based on Scorpio-Centaurus membership (Jones and Shobbrook 1974) are 0.4 mag fainter than those shown in Fig. 4. This adjustment brings many of the observed stars into agreement with the models, although some short periods do remain. These cases could represent the presence of nonradial oscillations (see Stamford and Watson 1977).

Values for $Q_0$ are also listed in Table I. They are in excellent agreement with Watson's (1972) derived value of $Q = 0.037$ for 18 observed stars using gravity data. Jones and Shobbrook (1974) find values in the range $Q = 0.025$–$0.040$ with most stars falling near $Q = 0.030$. Since $Q_1 \approx 0.026$, this places the stars midway between the fundamental and first-overtone modes. Some are probably fundamental pulsators, some may be in nonradial modes.

Multiple periods and beat periods have been observed in many cases. Since only one unstable mode has been found, the present mechanism does not account for this phenomenon. This may not be a serious objection, however, since similar unexplained beats occur in other types of variables, notably RR Lyrae stars, for which radial pulsations are clearly indicated.

Observed $\beta$ Cephei stars reach maximum light when the star is at minimum radius, as opposed to classical Cepheids which attain maximum luminosity one quarter cycle (90°) later than the time of minimum radius. The phase lags (in degrees, where 360° = 1 period) for the models computed here are shown in Table I. Negative lags mean that maximum light precedes minimum radius. It is seen that, although some variation is present, a zero phase lag, as observed, is the general rule near the instability region. This is the expected result for a purely adiabatic oscillator. The negative lags and the trend toward larger lags at hotter temperature (just opposite to the behavior of classical Cepheids) are not presently understood. The theory of Castor (1968) evidently does not apply, since it depends on the H ionization zone. It seems significant, however, that a similar tendency toward zero phase lag is found in early Cepheid models computed by Cox (1959, 1960, 1963). These models contained a single ($He^+$) ionization zone, and negative phase lags were produced by a dissipative region above this zone, as in model 4.1S (Fig. 1, Table I). These phase lags found by Cox also increase toward the blue as found here.

Also in Table I is the amplitude ratio $(\Delta R/R)/\Delta M_{\rm bol}$, shown by Watson (1971) to have a value of about 0.12 among observed $\beta$ Cepheids. The results found here are generally in agreement with the observed value. The observed light amplitudes are thus entirely consistent with radial pulsations, as noted by Watson, even though the $V$ amplitudes are very small. The quantity $(\Delta R/R)/\Delta M_{\rm bol}$, as well as the phase lag discussed above, could be modified by nonlinear atmospheric effects. More detailed models are required before an accurate comparison will be possible.

## V. CONCLUSIONS

In the preceding discussion a destabilization mechanism for $\beta$ Cephei stars has been demonstrated. Actual instability is not found in normal models, and this implies either (1) current physical data underestimate the strength of the effect, or (2) an additional destabilizing mechanism may be present. The second possibility could be linked to the widespread velocity variations found among early type stars (Smith 1977; Lucy 1976) probably indicative of nonradial modes. The two effects superposed may then account for the special characteristics of the $\beta$ Cepheids.

The models presented have periods, $Q$ values, phase lags, and light amplitudes in agreement with most observed variables. In particular, the low-amplitude variables (including $\gamma$ Peg, $\delta$ Cet, and $\zeta^1$CMa according to Stamford and Watson 1977) are probably radial pulsators. Nonradial modes may be present in other cases, accounting for several anomalously low periods.

The mechanism presented here is an envelope ionization mechanism similar to that responsible for the classical Cepheid strip. It is thus rather appealing by virtue of its simplicity. Important differences distinguish this case, however: The driving does not depend on an ionization zone—it is purely an opacity effect; the hydrogen ionization zone, so important in the Cepheid strip, is completely absent; and the central condensation of the models is much lower than that of Cepheids at similar luminosities. These differences certainly are responsible for the unusual behavior of the phase lag and the negative slope of the instability strip found here. Just how these consequences relate to the causes remains a problem for the future.

This research is supported by NSF Grant AST 77-26993 through Rutgers University. Thanks are extended to N. Baker for commenting on the original manuscript.

## REFERENCES

Aizenman, M., and Weigert, A. (1977). Astron. Astrophys. **56,** 457.

Baker, N. (1966). *Stellar Evolution,* edited by Stein and Cameron (Plenum, New York), p. 333.

Beardsley, W. R. (1978). Preprint.

Carson, T. R. (1976). Ann. Rev. Astron. Astrophys. **14,** 95.

Castor, J. P. (1968). Astrophys. J. **154,** 793.

Castor, J. P. (1971). Astrophys. J. **166,** 109.

Cox, A. N., and Tabor, J. E. (1974). *Stellar Instability and Evolution,* edited by Ledoux, Noels, and Rodgers, IAU Symp. No. 59 (Reidel, Dordrecht), p. 73.
Cox, A. N., and Tabor, J. E. (1976). Astrophys. J. Suppl., **31,** 271.
Cox, J. P. (1959). Astrophys. J. **130,** 296.
Cox, J. P. (1960). Astrophys. J. **137,** 594.
Cox, J. P. (1963). Astrophys. J. **138,** 487.
Cox. J. P. (1965). *Aerodynamic Phenomena in Stellar Atmospheres,* edited by Thomas, IAU Symp. No. 28 (Reidel, Dordrecht), p. 90.
Cox, J. P. (1976). *Proceedings of the Solar and Steliar Pulsation Conference,* edited by A. N. Cox and R. G. Deupree (LASL, Los Alamos), p. 127.
Cox, J. P., and Giuli, R. T. (1968). *Principles of Stellar Structure* (Gordon and Breach, New York).
Davey, W. P. (1973). Astrophys. J. **179,** 235.
Davis, C. G., and Davison, D. K. (1978). Astrophys. J. **221,** 929.
Dziembowski, W. (1978). Preprint.
Jones, D. H. P., and Shobbrook, R. R. (1974). Mon. Not. R. Astron. Soc. **166,** 649.
Lesh, J. R., and Aizenman, M. L. (1973a). Astron. Astrophys. **22,** 229.
Lesh, J. R., and Aizenman, M. L. (1973b). Astron. Astrophys. **26,** 1.
Lesh, J. R., and Aizenman, M. L. (1974). Astron. Astrophys. **34,** 203.
Lesh, J. R., and Aizenman, M. L. (1975). *Multiple Periodic Variable Stars* IAU Colloquium No. 29 (Reidel, Dordrecht), p. 11.
Lucy, L. B. (1976). Astrophys. J. **206,** 499.
Magee, N. H., Merts, A. L., and Huebner, W. F. (1975). Astrophys. J. **196,** 617.
Osaki, Y. (1976). Publ. Astron. Soc. Jpn. **28,** 105.
Sareyan, J. P., Le Contel, J. M., Valtier, J. C., and Ducatel, D. (1978). Preprint.
Smith, M. A. (1977). Astrophys. J. **215,** 574.
Stamford, P. A., and Watson, R. D. (1977). Mon. Not. R. Astron. Soc. **180,** 551.
Stellingwerf, R. F. (1975a). Astrophys. J. **195,** 441.
Stellingwerf, R. F. (1975b). Astrophys. J. **199,** 705.
Stellingwerf, R. F. (1976). *Proceedings of the Solar and Stellar Pulsation Conference,* edited by A. N. Cox and R. G. Deupree (LASL, Los Alamos), p. 181.
Stellingwerf, R. F. (1978). Astrophys. J. (in press).
Stothers, R. (1976a). Astrophys. J. **204,** 853.
Stothers, R. (1976b). Astrophys. J. **210,** 434.
Underhill, A. (1966). *The Early-type Stars* (Reidel, Dordrecht), Chap. 16.
Van Hoof, A. (1970). *Spectroscopic Astrophysics,* edited by G. H. Herbig (Univ. Calif. P., Berkeley), p. 343.
Watson, R. D. (1971). Astrophys. J. **170,** 345.
Watson, R. D. (1972). Astrophys. J. Suppl. **24,** 167.